Geomechanics and Engineering, *Vol. 34, No. 1 (2023) 43-49*
https://doi.org/10.12989/gae.2023.34.1.043

LSTM algorithm to determine the state of minimum horizontal stress during well logging operation

Arsalan Mahmoodzadeh*[1], Seyed Mehdi Seyed Alizadeh[2a], Adil Hussein Mohammed[3b], Ahmed Babeker Elhag[4c], Hawkar Hashim Ibrahim[5d] and Shima Rashidi[6e]

[1]*Department of Civil Engineering, University of Halabja, Halabja, Kurdistan Region, Iraq*
[2]*Petroleum Engineering Department, Australian University, West Mishref, Kuwait*
[3]*Department of Communication and Computer Engineering, Faculty of Engineering, Cihan University-Erbil, Kurdistan Region, Iraq*
[4]*Department of Civil Engineering, College of Engineering, King Khalid University, Abha 61413, Saudi Arabia*
[5]*Department of Civil Engineering, College of Engineering, Salahaddin University-Erbil, 44002 Erbil, Kurdistan Region, Iraq*
[6]*Department of Computer Science, College of Science and Technology, University of Human Development, Sulaymaniyah, Kurdistan Region, Iraq*

(*Received October 16, 2022, Revised May 8, 2023, Accepted May 10, 2023*)

Abstract. Knowledge of minimum horizontal stress (S_{hmin}) is a significant step in determining full stress tensor. It provides crucial information for the production of sand, hydraulic fracturing, determination of safe mud weight window, reservoir production behavior, and wellbore stability. Calculating the S_{hmin} using indirect methods has been proved to be awkward because a lot of data are required in all of these models. Also, direct techniques such as hydraulic fracturing are costly and time-consuming. To figure these problems out, this work aims to apply the long-short-term memory (LSTM) algorithm to S_{hmin} time-series prediction. 13956 datasets obtained from an oil well logging operation were applied in the models. 80% of the data were used for training, and 20% of the data were used for testing. In order to achieve the maximum accuracy of the LSTM model, its hyper-parameters were optimized significantly. Through different statistical indices, the LSTM model's performance was compared with with other machine learning methods. Finally, the optimized LSTM model was recommended for S_{hmin} prediction in the well logging operation.

Keywords: long-short-term memory; machine learning; minimum horizontal stress; optimization; well logging

1. Introduction

Fracture mechanics is the field of mechanics concerned with the study of the propagation of cracks in materials (Zhang *et al.* 2022a, Zhao *et al.* 2023, Li *et al.* 2023). It uses methods of analytical solid mechanics to calculate the driving force on a crack and those of experimental solid mechanics to characterize the material's resistance to fracture (Xiao *et al.* 2023, Xia *et al.* 2022, Wu *et al.* 2022). Today, fracture analysis of various materials such as rock, concrete, cement, steel, etc., which various engineering projects deal with, has a special place in the science of fracture mechanics (Zhang and Abedini 2022, Zhang *et al.* 2023, Huang *et al.* 2023). For this purpose, today many researchers are trying to provide different methods and strengthen them as much as possible to examine these materials (Zhang *et al.* 2022b, Zhang *et al.* 2022c, Liu *et al.* 2023a). One of the most important of these cases is the examination of rock fracture using the hydraulic fracturing method in a well logging operation. Investigating rock as a natural material has many complications. The properties of a particular rock type vary under different conditions (Yang *et al.* 2022a, b). One of the most important characteristics of rocks in various projects is the level of stress tolerance. In many phases of oil and gas exploration and production, the mechanical properties of rock formation along with such in-situ stress field as principal stress magnitudes and directions are essential parameters to be measured (Yu *et al*. 2021, Ren *et al.* 2022a). The in-situ minimum horizontal stress (S_{hmin}) is an important reservoir stress to take into account for reservoir stimulation techniques including hydraulic fracturing design and reservoir stability analysis (e.g., evaluation of wellbore stability during drilling and evaluation of sanding potential of reservoir sand) (Peng *et al.* 2022, Hong *et al.* 2023). Despite the importance of getting S_{hmin} right, it has long been recognized as the hardest part of the stress tensor to calculate (Li *et al.* 2022a, Jin *et al.* 2022, Xiao *et al.* 2022).

The size of the in-situ S_{hmin} is often estimated using both indirect and direct method (Mohammed *et al.* 2018,

∗Corresponding author, M.Sc.
E-mail: arsalan.mahmoodzadeh@uoh.edu.iq
[a]Ph.D.
E-mail: s.alizadeh@au.edu.kw
[b]M.Sc.
E-mail: adil.mohammed@cihanuniversity.edu.iq
[c]Ph.D.
E-mail: abalhaj@kku.edu.sa
[d]M.Sc.
E-mail: hawkar.ibrahim@su.edu.krd
[e]M.Sc.
E-mail: shima.rashid@uhd.edu.iq

ISSN: 2005-307X (Print), 2092-6219 (Online)

Dahab *et al.* 2020). S_{hmin} estimate suffers from unfortunate ambiguity in most circumstances (Hayavi and Abdideh 2016). The indirect methods have been represented by a number of models, such as those developed by Terzaghi, Anderson, Newberry, Huang, and the horizontal poroelastic strain (Najibi *et al.* 2017). A reliable estimate for the minimum in-situ stress, however, has proven difficult to calculate because all of these models require a large amount of data, including the core data, the overburden stress, the pore pressure, the static Young's modulus, the Poisson's ratio, and the shear sonic transit time (Song and Hareland 2012).

Nevertheless, other tests, such hydraulic fracturing and/or hydraulic testing of preexisting fractures, use direct stress measurements, which is how direct techniques get their name (Li *et al.* 2009). The International Society for Rock Mechanics (ISRM) has recommended this technique as a reliable way for estimating rock stress at depths of several thousand meters from the surface (Haimson and Cornet 2003). These methods can be effective, but they are time-consuming, expensive, and need specialized test equipment and knowledgeable workers to carry them successfully. The conventional leak-off test (LOT) and extended leak-off test (XLOT) have been used to establish the minimum in-situ stress magnitude because of their similarity to the small volume hydraulic fracturing technique (Gjønnes *et al.* 1998). The LOT and XLOT processes were created by the drilling industry and are widely employed in exploratory wells when the formation characteristics are unknown. The primary objectives of such tests are to calculate the strength or fracture pressure of the open formation and to determine the upper limit of the mud weight so that the next section of the open borehole may be drilled. After a mechanistic evaluation, it was accepted as a method for measuring stress. On the other hand, there is a limit on the number of data points that can be covered by the LOT and XLOT methods at any given level of detail. The geophysical well log is a useful technique for predicting in-situ S_{hmin} in continuous profiles throughout the whole reservoir interval for two main reasons. To start, wireline logs offer direct measurements of the rock's petrophysical parameters. Moreover, the wireline log is one of the few downhole measurements that may be taken across the whole reservoir. Nevertheless, the S_{hmin} cannot be determined using wireline records. The use of artificial intelligence methods is a practical answer to these problems (Zhang *et al.* 2022d). Since many of the same characteristics that define in-situ S_{hmin} also impact other physical attributes like velocity, density, and porosity, this answer has some context.

Artificial intelligence techniques may learn the pattern or behavior of the prior experience via sets of training data without the necessary comprehensive explanation of the underlying physics (Liu *et al.* 2021, Mahmoodzadeh *et al.* 2022, Xiang *et al.* 2021, Bai *et al.* 2021, Han *et al.* 2021, Pan *et al.* 2021). It's crucial to remember that the best artificial intelligence approach is one that takes into account the specifics of the data at hand and the task at hand (Ren *et al.* 2022b, Liu *et al.* 2023b, Li *et al.* 2020). The ability of these methods has been proven in many fields (Li *et al.* 2022b, Zhan *et al.* 2022, Zhan *et al.* 2023). For the problem of S_{hmin} in well drilling operations, the S_{hmin} responses from different time steps (different depths) are generally related. As in literature, recurrent neural networks (RNNs) such as long-short-term memory (LSTM) are proper for predictions based on time-series data (Salman *et al.* 2018, Zhang *et al.* 2018) even when there are time lags between events (Chen *et al.* 2016). This could be an advantage for the prediction of S_{hmin}.

In this work, the LSTM method was optimized to S_{hmin} time-series prediction. For this purpose, 13956 datasets obtained from an oil exploration hole with a depth of 4066 meters were considered in the models. 80% of the data were used for training, and 20% of the data collected from the bottom of the hole were used for testing. The potential of the LSTM model was evaluated using statistical indices. Also the prediction performance of the optimized LSTM model was compared with eight other machine learning techniqes. Finally, the robustness of different models was discussed.

2. LSTM algorithm

Using the cell's state storage, the LSTM cell's memory is transformed from input to output (Hochreiter and Schmidhuber 1997). The general construction of the LSTM cell is shown in Fig. 1. There are four gates in an LSTM cell: an input, an update, a forget, and an output. In further detail, the input gate chooses what to take into the neuron and how, the forget gate chooses what to remove from the previous memory cells, the update gate alters the cell, and the output gate creates the new long-term memory. Each of the LSTM's four fundamental parts will function differently, taking in inputs such as input series and long- and short-term memories at a particular time step and producing new memories and outputs at the same time step. An input gate computes the information that has to be transmitted to the cell, which is mathematically stated as (Graves 2012)

$$in(t) = \psi(W_{in} \times \big(x(t), hs(t-1)\big) + \theta_{in}) \quad (1)$$

The vectors' individual components are multiplied using operator "×".

The forget gate is a mathematically modelable system that decides how much previous memory is forgotten.

$$fg(t) = \psi(W_{fg} \times \big(x(t), hs(t-1)\big) + \theta_{fg}) \quad (2)$$

How the update gate affects a cell's state may be represented by a series of equations

$$\tilde{c}_s(t) = \tanh(W_{c_s} \times \big(x(t), hs(t-1)\big) + \theta_{c_s}) \quad (3)$$

$$c_s(t) = fg(t) \times c_s(t-1) + in(t) \times \tilde{c}_s(t) \quad (4)$$

The output gate, which is in charge of making changes to the output, modifies the hidden layer from the previous time step in the manner defined by

$$og(t) = \psi(W_{og} \times \big(x(t), hs(t-1)\big) + \theta_{og}) \quad (5)$$

$$hs(t) = og(t) \times \tanh(c_s(t)) \quad (6)$$

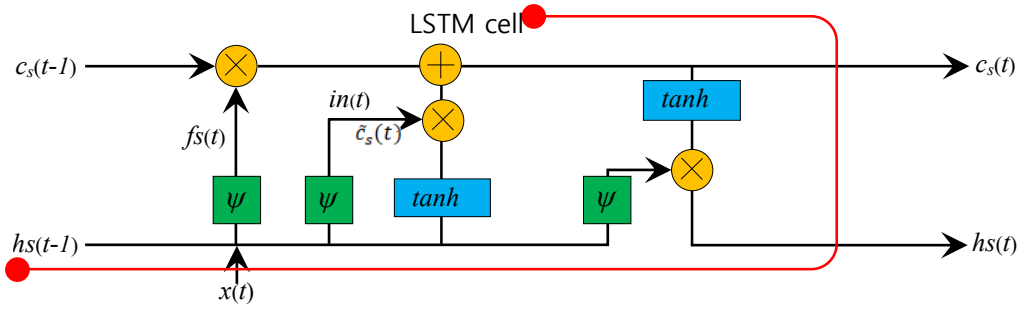

Fig. 1 Overall structure of typical LSTM cell

3. Database

13956 datasets obtained from a vertical well logging operation in the understudied area from depth 1936 m to depth 4066m, including depth (D) and S_{hmin} were utilized in this study. 11164 datasets (80% of all data) were used for training and 2792 datasets (20% of all data) for test.

4. Statistical evaluation indices

To evaluate the accuracy of the forecasting models, some statistical evaluation indices, including coefficient of determination (R^2), root mean square error (RMSE), mean absolute error (MAE), and mean absolute percentage error (MAPE), are taken into account. The following formulas for calculating these indices are presented (Eqs. (7)-(10)).

$$R^2 = 1 - \frac{sum\ squared\ regression\ (SSR)}{sum\ of\ squares\ total\ (SST)} \tag{7}$$

$$\text{MAE} = \left(\frac{1}{n}\right)\sum_{i=1}^{n}|y_i - y_i'| \tag{8}$$

$$\text{MAPE} = \frac{1}{n}\sum_{i=1}^{n}\left|\frac{y_i - y_i'}{y_i}\right| \times 100\% \tag{9}$$

$$\text{RMSE} = \sqrt{\left(\frac{1}{n}\right)\sum_{i=1}^{n}(y_i - y_i')^2} \tag{10}$$

where y_i is the actual value, y_i' is the predicted value, $\bar{y}_i$ and $\bar{y}_i'$ are the means of actual and predicted values, and n is the number of samples.

5. Development of neural networks

5.1 Normalization method

The key work of ML is data normalization. Variations in size and units are commonplace because of the wide variety of data sources. Normalization of training data may help models converge more quickly with fewer mistakes. The data in this study are standardized to a range of zero to one using the Min-Max normalization method (see Eq. (11)).

$$x_{(0,1)} = \frac{x - Min}{Max - Min} \tag{11}$$

where x and $x_{(0,1)}$ stand for the raw data and its normalized version, respectively, and Min and Max stand for the smallest and largest values in the complete dataset, which includes both training and testing data. Min-max normalization is frequently used and successful in the literature. Adding additional data may need re-normalization if the range of values is expanded, which is the main drawback of this normalizing procedure. Fixing the aforementioned issue requires making the Min-Max range somewhat wider than the extremes of the original data. This ensures that any future data will always be contained inside the specified Min-Max range.

5.2 Model optimization

The codes of this work were developed in Python using the Tensorflow package, which provides a high-level programming interface for neural networks. The computation was carried out on an Intel(R) Core (TM) i7-10750H CPU running at 2.60 GHz with 32 GB of RAM.

Speeding up training and improving prediction accuracy both depend on optimizing models, which is inextricably tied to the process of identifying hyperparameters. Researching various parameter values yields the best results. Experiments are conducted to determine the optimal ranges for the parameters epoch numbers, hidden neurons, batch size, and input time series length. Based on the R^2 and RMSE, the best hyperparameters may be determined.

Next, we'll describe the steps we need to take to determine the best possible epoch number. For the span of epochs, many epochs are picked and compared (Table 1). Keep in mind that the other settings are kept fixed (batch size = 32, activation function = tanh, time-series length = 1, hidden neurons = 32, hidden layers = 3). Table 1 shows the R^2 and RMSE values achieved by the LSTM model throughout the testing period using different numbers of training epochs. Initially, when the epoch number is increased, R^2 increases but RMSE decreases. At this stage, the accuracy begins to drop, which is indicative of an overfitting problem. According to Table 1, 700 epochs is the

Table 1 The R2 and RMSE results for the testing period with various training epochs

Epoch	R^2	RMSE
100	0.8342	0.112
200	0.8518	0.107
400	0.9037	0.091
500	0.9155	0.086
600	0.9231	0.082
700	0.9322	0.078
800	0.9224	0.083
900	0.9142	0.086

Table 2 The R^2 and RMSE results for the testing period using the RNN models with various training batch_size

batch_size	R^2	RMSE
8	0.9427	0.068
16	0.9269	0.075
32	0.9322	0.078
64	0.9136	0.081
128	0.8595	0.098

Table 3 The R^2 and RMSE results for the testing period using the RNN models with various activation functions

Activation function	R^2	RMSE
tanh	0.9427	0.068
ReLU	0.9588	0.037
Linear	0.9584	0.038
Sigmoid	0.8745	0.087
SELU	0.9581	0.036
Exponential	0.9474	0.052

sweet spot. The epoch numbers will be used as a fixed input in the following procedures (equal to 700). Altering the LSTM's parameters, either their type or values, can allow for a better model to be accessed.

Batch_size is a term utilized in ML and refers to the number of training examples used in repetition. The outcomes of the testing period for a variety of batch_size numbers are summarized in Table 2. The largest R^2 and the smallest RMSE values are yielded by 8 batch_size. Therefore, the optimum number of batch_size is considered equal to 8.

Regarding the activation functions in the output layer, varieties of commonly-used activation functions are analyzed, including linear, sigmoid, exponential, SELU (scaled exponential linear unit), tanh, and ReLU (rectified linear unit). The outcomes of the testing period are summarized in Table 3. The ReLU function yields the largest R^2 and the smallest RMSE. So, the ReLU activation function (Eq. (12)) can be appropriate for this study.

$$ReLu(x) = \begin{cases} x, & x > 0 \\ 0, & x \leq 0 \end{cases} \quad (12)$$

Table 4 The R^2 and RMSE results for the testing period using the RNN models with various time series length

L_s	R^2	RMSE
1	0.9588	0.037
2	0.9638	0.055
3	0.9691	0.046
4	0.9626	0.057
5	0.9789	0.046
6	0.9859	0.012
7	0.9786	0.044
8	0.9612	0.051

The size of input time series data is determined by the length of the sliding window (denoted as L_s in this study). For example, if the recorded time series data frequency is 1 meter and L_s=10, the RNNs will be trained to predict the S_{hmin} at the next meter using data from every 10 meters. As shown in Table 4, the LSTM model is trained with various values of L_s so that the effect of L_s on the model performance can be studied. According to Table 4, the largest R^2 and the smallest RMSE produced by the LSTM model are yielded by L_s = 6. So, the optimum value for L_s is 6.

In order to improve prediction accuracy or solve more complicated problems, multi-layer models are often considered. Till now, the LSTM model has used 3 hidden layers. The model was evaluated with one, two, three, and four hidden layers to see how the number of hidden layers affects the prediction outcomes. A comparison between the results of single-layer and multi-layer models indicated that, in terms of R^2 and RMSE, raising the hidden layers from one to three improves the results. There was no improvement in the results for the four-layer model, and there was also a minor drop in the accuracy of the results. For that reason, for the optimal LSTM model, the three-layer model was considered. Also, the consumed time was increased with the number of hidden layers increment.

The model's accuracy was also investigated by various hidden neurons [8, 16, 32, 64, 128]. For hidden neurons = 32, the most robust results were produced by the LSTM model. Also, the optimization algorithm used was the Nesterov-accelerated adaptive moment estimation (Nadam). Finally, the obtained optimal hyper-parameters are as follows: 700 epochs, 32 hidden neurons, 8 batch_size, 3 hidden layers, ReLU activation function, L_3=6, and Nadam optimization algorithm.

6. Results and discussion

All the statistical evaluation indices results for the LSTM model are presented in Table 5 for the training datasets. The R^2 value of the model is 0.9987, indicating that the optimized model can achieve high training effects.

After the model training was completed, the testing datasets (20% of data) were utilized to verify and evaluate the model. The S_{hmin} predictions made by the LSTM model

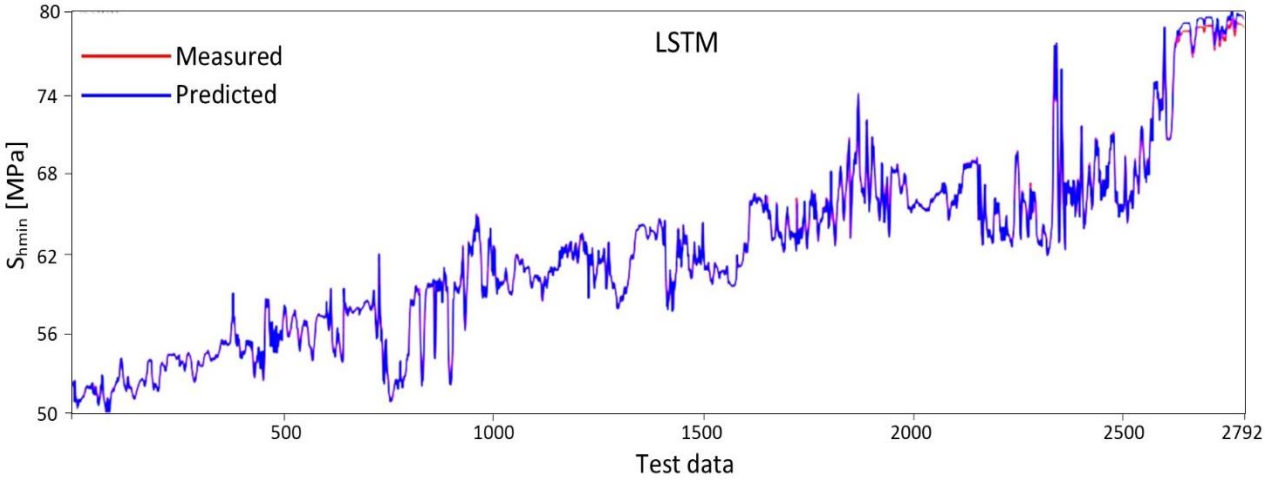

Fig. 2 Comparison of the measured and predicted reslts

	GRU	LSTM	RNN	ANN	GPM	SVM	ANFIS	KNN	DT
R2	0.9963	0.9859	0.9655	0.9312	0.8857	0.8592	0.843	0.8213	0.8046
MAE	0.9921	0.991	0.9751	0.9578	0.9218	0.9079	0.8969	0.8796	0.86943
MAPE	0.992101	0.990902	0.975038	0.9578	0.9218	0.9079	0.8969	0.8796	0.86943
RMSE	0.994	0.988	0.969	0.9278	0.8918	0.8779	0.8669	0.8496	0.83943

Fig. 3 Accuracy matrix to analyze the performance of the ML models in the prediction of S_{hmin}

are shown in Fig. 2 and compared with the measured ones. As in Fig. 2, the optimized LSTM model has presented accurate results. The statistical indices results for the testing data are also presented in Table 5.

In addition to the LSTM model, the prediction performance of eight other models to predict the Shmin including recurrent neural networks (RNN), gated recurrent unit (GRU), Gaussian process machine (GPM), adaptive neuro fuzzy inference system (ANFIS), decision trees (DT), support vector machine (SVM), K-nearest neighbors (KNN), and artificial neural network (ANN) are also examined by this study using. In Fig. 3, to evaluate the developed models' performance, the statistical evaluation indicators are displayed through a recently proposed thermal map matrix called the accuracy matrix. Considering the ideal value as a reference, the accuracy obtained by the developed models for each performance index is calculated. For example, the ideal values for R2 and MAE, MAPE, and RMSE are 1, 0, 0, and 0, respectively. In this study, for the GRU model, these values were obtained by about 0. 0.9963, 0.0079, 0.7899, and 0.006, respectively, in the testing phase. Hence, the GRU model's accuracy is calculated as 0.9963% (0.9963/1 = 0.9963), 0.9921% (1-0.0079 = 0.9921), 0.9921% ((100 - 0.7899)/100 = 0.9921), and 0.9940% (1 – 0.006 = 0.9940), respectively, in terms of R2, MAE, MAPE, and RMSE. As in Fig. 3, the performance predictions of the models to predict the Shmin from high to low are GRU, LSTM, RNN, ANN, GPM, SVM, ANFIS, KNN, and DT, respectively

Table 5 Statistical indices results

Data	R^2	MAE	MAPE	RMSE
Training	0.9987	0.0025	0.2507	0.006
Test	0.9859	0.0090	0.9098	0.012

7. Conclusions

The obtained results in this study lead to the following conclusions:

- Considering the datasets used in this study, the optimal hyper-parameters for the LSTM model were obtained as follows: 700 epochs, 32 hidden neurons, 8 batch_size, 3 hidden layers, ReLU activation function, L_3=6, Nadam optimization algorithm, and 0.5 dropout rate.
- The R^2 value of the LSTM for the testing and training phases were 0.9859 and 0.9987, respectively.

- The performance prediction of several ML models to predict the S_{hmin} were ordered as follows: GRU, LSTM, RNN, ANN, GPM, SVM, ANFIS, KNN, and DT.
- Applying extra hidden layers in the structural network prolongs the training period.

Acknowledgements

The authors extend their appreciation to the Deanship of Scientific Research at King Khalid University for funding this work through large group Research Project under grant number RGP2/357/44.

References

Al-Baiyat, I.A. and Heinze, L. (2012.),"Implementing artificial neural networks and support vector machines in stuck pipe prediction", Proceedings of the SPE Kuwait International Petroleum Conference and Exhibition, Kuwait City, Kuwait, 10-12, December. https://doi.org/10.2118/163370-ms.

Chen, Y., Zhong, K., Zhang, J., Sun, Q. andZhao, X.L. (2016), "LSTM networks for mobile human activity recognition", *Proceedings of the International Conference on Artificial Intelligence: Technologies and Applications. ICAITA*, https://doi.org/10.2991/icaita-16.2016.13

Dahab, A.S., Abdulaziz, A.M., Manhalawi, A., Abbas, A.K. and AL-Husseini, N. (2020), "Managing wellbore instability through geomechanical modeling and wellbore stability analysis", *Proceedings of the 54th US Rock Mechanics/Geomechanics Symposium (ARMA)*, Golden, Colorado, USA, 28 June-1 July, Paper No. ARMA 20-1378.

Gjønnes, M., Cruz, A.M., Horsrud, P. and Holt, R.M. (1998), "Leak-off tests for horizontal stress determination", *J. Petroleum Sci. Eng*., **20**(1-2), 63-71. https://doi.org/10.1016/s0920-4105(97)00053-3.

Graves, A. (2012). "Long short-term memory. In Supervised sequence labelling with recurrent neural networks", Springer-Verlag GmbH Berlin Heidelberg, 37-45. https://doi.org/10.1007/978-3-642-24797-2.

Hayavi, M.T. and Abdideh, M. (2016), "Estimation of insitu horizontal stresses using the linear poroelastic model and minifrac test results in tectonically active area", *Russian J. Earth Sci*., **16**, 1-9. https://doi.org/10.2205/2016ES000576.

Hochreiter, S. and Schmidhuber, J. (1997), "Long short-term memory", *Neural Comput.*, **9**, 1735-1780. https://doi.org/10.1162/neco.1997.9.8.1735.

Haimson, B. and Cornet, F. (2003), "ISRM suggested methods for rock stress estimation—Part 3: Hydraulic fracturing (HF) and/or hydraulic testing of preexisting fractures (HTPF)", *Int. J. Rock Mech. Min. Sci.*, **40**(7-8), 1011-1020. https://doi.org/10.1016/j.ijrmms.2003.08.002.

Han, W., Jiang, Y., Zhang, X., Koga, D. and Gao, Y. (2021), "Quantitative assessment on the reinforcing behavior of the CFRP-PCM method on tunnel linings", *Geomech. Eng*., **25**(2), 123-134. https://doi.org/10.12989/gae.2021.25.2.123.

Huang, Y., Huang, J., Zhang, W. and Liu, X. (2023), "Experimental and numerical study of hooked-end steel fiber-reinforced concrete based on the meso- and macro-models", *Compos. Struct*., 116750. https://doi.org/10.1016/j.compstruct.2023.116750.

Hong, Y., Yao, M. and Wang, L. (2023), "A multi-axial bounding surface p-y model with application in analyzing pile responses under multi-directional lateral cycling", *Comput. Geotech*., **157**, 105301. https://doi.org/10.1016/j.compgeo.2023.105301.

Jin, J., Zhang, X., Liu, X., Li, Y. and Li, S. (2022), "Study on critical slowdown characteristics and early warning model of damage evolution of sandstone under freeze-thaw cycles", *Front. Earth Sci*.. https://doi.org/10.3389/feart.2022.1006642.

Li, G., Lorwongngam, A. and Roegiers, J. (2009), "Critical review of leak-off test as a practice for determination of in-situ stresses", *Proceedings of the 43rd US Rock Mechanics Symposium and 4th U.S.-Canada Rock Mechanics Symposium*, Asheville, NC June 28th – July 1, Paper No. ARMA09-003.

Liu, J., Jiang, Y., Zhang, Y. and Sakaguchi, O. (2021), "Influence of different combinations of measurement while drilling parameters by artificial neural network on estimation of tunnel support patterns", *Geomech. Eng*., **25**(6), 439-454. https://doi.org/10.12989/gae.2021.25.6.439.

Liu, H., Chen, Z., Liu, Y., Chen, Y., Du, Y. and Zhou, F. (2023a), "Interfacial debonding detection for CFST structures using an ultrasonic phased array: Application to the Shenzhen SEG building", *Mech. Syst. Signal Pr*., **192**, 110214. https://doi.org/10.1016/j.ymssp.2023.110214.

Li, X., Du, C., Wang, X. and Zhang, J. (2023), "Quantitative determination of high-order crack fabric in rock plane", *Rock Mech. Rock Eng*., https://doi.org/10.1007/s00603-023-03319-x.

Li, R., Wu, X., Tian, H., Yu, N. and Wang, C. (2022b), "Hybrid memetic pretrained factor analysis-based deep belief networks for transient electromagnetic Inversion", *IEEE T. Geosci. Remote*, **60**. https://doi.org/10.1109/TGRS.2022.3208465.

Li, X. and Sun, Y. (2020), "Stock intelligent investment strategy based on support vector machine parameter optimization algorithm", *Neural Comput. Appl*., **32**(6), 1765-1775. https://doi.org/10.1007/s00521-019-04566-2.

Li, R., Zhang, H., Chen, Z., Yu, N., Kong, W., Li, T. and Liu, Y. (2022a), "Denoising method of ground-penetrating radar signal based on independent component analysis with multifractal spectrum", *Measurement*, **192**, 110886. https://doi.org/10.1016/j.measurement.2022.110886.

Liu, H., Yue, Y., Liu, C., Spencer, B.F. and Cui, J. (2023b), "Automatic recognition and localization of underground pipelines in GPR B-scans using a deep learning model", *Tunn. Undergr. Sp. Tech*., **134**, 104861. https://doi.org/10.1016/j.tust.2022.104861

Mohammed, H.Q,, Abbas, A.K. and Dahm, H.H. (2018), "Wellbore instability analysis for Nahr Umr formation in Southern Iraq", *Proceedings of the 52nd US Rock Mechanics/Geomechanics Symposium (ARMA)*, Seattle, Washington, June 17-20, Paper No. ARMA 18–916.

Mahmoodzadeh, A., Rashidi, S., Mohammed, A., Hama Ali, H. and Ibrahim, H. (2022), "Machine learning approaches to enable resource forecasting process of road tunnels construction", *Commun. Eng. Comput. Sci.*, https://conferences.cihanuniversity.edu.iq/index.php/COCOS/22/paper/view/718.

Najibi, A.R., Ghafoori, M., Lashkaripour, G.R. and Asef, M.R. (2017), "Reservoir geomechanical modeling: Insitu stress, pore pressure, and mud design", *J. Petroleum Sci. Eng*., **151**, 31-39. https://doi.org/10.1016/j.petrol.2017.01.045

Pan, Q., Chen, Z., Wu, Y., Dias, D. and Oreste, P. (2021), "Probabilistic tunnel face stability analysis: A comparison between LEM and LAM", *Geomech. Eng*., **24**(4), 399-406. https://doi.org/10.12989/gae.2021.24.4.399.

Peng, J., Xu, C., Dai, B., Sun, L., Feng, J. and Huang, Q. (2022), "Numerical investigation of brittleness effect on strength and microcracking behavior of crystalline rock", *Int. J. Geomech*., **22**(10), 4022178. https://doi.org/10.1061/(ASCE)GM.1943-5622.0002529.

Ren, C., Yu, J., Liu, S., Yao, W., Zhu, Y. and Liu, X. (2022a), "A plastic strain-induced damage model of porous rock suitable for

different stress paths", *Rock Mech. Rock Eng*., **55**(4), 1887-1906. https://doi.org/10.1007/s00603-022-02775-1.

Ren, Y., Jiang, H., Ji, N. and Yu, H. (2022b), "TBSM: A traffic burst-sensitive model for short-term prediction under special events", *Knowledge-Based Systems*, **240**, 108120. https://doi.org/10.1016/j.knosys.2022.108120

Song, L. and Hareland, G. (2012), "Minimum horizontal stress profile from logging data for Montney Formation of North East British Columbia", *Proceedings of the SPE Canadian Unconventional Resources Conference*, https://doi.org/10.2118/162233-ms

Salman, A.G., Heryadi, Y., Abdurahman, E. and Suparta, W. (2018), "Single layer & multi-layer long short-term memory (LSTM) model with intermediate variables for weather forecasting", *Procedia Comput. Sci*., **135**, 89-98. https://doi.org/10.1016/j.procs.2018.08.153.

Wu, Z., Xu, J., Li, Y. and Wang, S. (2022), "Disturbed state concept–based model for the uniaxial strain-softening behavior of fiber-reinforced soil", *Int. J. Geomec*h., **22**(7), 4022092. https://doi.org/10.1061/(ASCE)GM.1943-5622.0002415.

Xiao, X., Zhang, Q., Zheng, J. and Li, Z. (2023), "Analytical model for the nonlinear buckling responses of the confined polyhedral FGP-GPLs lining subjected to crown point loading", *Eng. Struct*., **282**, 115780. https://doi.org/10.1016/j.engstruct.2023.115780.

Xia, Y., Shi, M., Zhang, C., Wang, C., Sang, X., Liu, R. and Fang, H. (2022), "Analysis of flexural failure mechanism of ultraviolet cured-in-place-pipe materials for buried pipelines rehabilitation based on curing temperature monitoring", *Eng. Fai. Anal*., **142**, 106763. https://doi.org/10.1016/j.engfailanal.2022.106763.

Xiang, G., Ying, D., Gao, C. and Yuan, L. (2021), "Application of artificial neural network for prediction of flow ability of soft soil subjected to vibrations", *Geomech. Eng*., **25**(5), 395-403. https://doi.org/10.12989/gae.2021.25.5.395.

Xiao, D., Hu, Y., Wang, Y., Deng, H., Zhang, J., Tang, B. and Li, G. (2022), "Wellbore cooling and heat energy utilization method for deep shale gas horizontal well drilling", *Appl. Therm. Eng*., **213**, 118684. https://doi.org/10.1016/j.applthermaleng.2022.118684

Yang, J., Fu, LY., Zhang, Y., and Han, T., (2022a). "Temperature- and Pressure-Dependent Pore Microstructures Using Static and Dynamic Moduli and Their Correlation", Rock Mech Rock Eng., **55**, 4073-4092. https://doi.org/10.1007/s00603-022-02829-4

Yang, J., Fu, L., Fu, B., Deng, W. and Han, T. (2022b), "Third-order padé thermoelastic constants of solid rocks", J. *Geophys. Research: Solid Earth*, **127**(9), e2022J-e24517J. https://doi.org/10.1029/2022JB024517.

Yu, J., Zhu, Y., Yao, W., Liu, X., Ren, C., Cai, Y. and Tang, X. (2021), "Stress relaxation behaviour of marble under cyclic weak disturbance and confining pressures", *Measurement*, **182**, 109777. https://doi.org/10.1016/j.measurement.2021.109777.

Zhang, J., Zhu, Y., Zhang, X., Ye, M. and Yang, J. (2018), "Developing a Long Short-Term Memory (LSTM) based model for predicting water table depth in agricultural areas", *J. Hydrol*., **561**, 918-929. https://doi.org/10.1016/j.jhydrol.2018.04.065.

Zhao, B., Wang, G., Wu, B. and Kong, X. (2023), "A study on mechanical properties and permeability of steam-cured mortar with iron-copper tailings", *Constr. Build. Mater*., **383**, 131372. https://doi.org/10.1016/j.conbuildmat.2023.131372.

Zhang, W., Kang, S., Huang, Y. and Liu, X. (2023), "Behavior of reinforced concrete beams without stirrups and strengthened with basalt fiber–reinforced polymer sheets", *J. Compos. Constr*., **27**(2), 4023007. https://doi.org/10.1061/JCCOF2.CCENG-4082.

Zhang, C. and Abedini, M. (2022), "Application of Lagrangian approach to generate P-I diagrams for RC columns exposed to extreme dynamic loading", *Adv. Concrete Constr*., **14**(3), 153-167. https://doi.org/10.12989/acc.2022.14.3.153.

Zhang, X., Ma, F., Dai, Z., Wang, J., Chen, L., Ling, H. and Soltanian, M.R. (2022a), "Radionuclide transport in multi-scale fractured rocks: A review", *J. Hazard. Mater*., **424**, 127550. https://doi.org/10.1016/j.jhazmat.2021.127550.

Zhang, H., Ouyang, Z., Li, L., Ma, W., Liu, Y., Chen, F. and Xiao, X. (2022b), "Numerical dtudy on welding residual stress distribution of corrugated steel webs", *Metals*, **12**(11), 1831. https://doi.org/10.3390/met12111831.

Zhang, X., Wang, Z., Reimus, P., Ma, F., Soltanian, M.R., Xing, B. and Dai, Z. (2022c), "Plutonium reactive transport in fractured granite: Multi-species experiments and simulations", *Water Res.*, **224**, 119068. https://doi.org/10.1016/j.watres.2022.119068.

Zhang, Q., Ge, L., Hensley, S., Isabel Metternicht, G., Liu, C. and Zhang, R. (2022d), "PolGAN: A deep-learning-based unsupervised forest height estimation based on the synergy of PolInSAR and LiDAR data", *ISPRS J. Photogrammetry Remote Sens*., **186**, 123-139. https://doi.org/10.1016/j.isprsjprs.2022.02.008.

Zhan, C., Dai, Z., Soltanian, M.R. and de Barros, F.P.J. (2022), "Data-worth analysis for heterogeneous subsurface structure identification with a stochastic deep learning framework", *Water Resour. Res*., https://doi.org/10.1029/2022WR033241.

Zhan, C., Dai, Z., Yang, Z., Zhang, X., Ma, Z., Thanh, H.V. and Soltanian, M.R. (2023), "Subsurface sedimentary structure identification using deep learning: A review", *Earth-Sci. Rev*., **239**, 104370. https://doi.org/10.1016/j.earscirev.2023.104370.

IC